Determining Fabry-Pérot Cavity Length Using White Light Interfereometry

Yangou Du[a,b,1] **and Joel Sabot**[a,b,2]

[a]Supervisor: Lilian Childress; [b]McGill University Department of Physics; [1]ID:260828040; [2]ID: 260822643

This manuscript was compiled on January 16, 2024

White light interferometery can be useful to measure lengths, and has applications in Cavity Quantum Electrodynamics where microcavity properties need to be measured. It is difficult to determine the length of these cavities, as errors in direct geometrical measurements are typically large. With this project, the goal is to determine the length of a Fabry-Pérot cavity accurately with a proposed white light interferometery technique. The interferometer is compared with a piezoelectric drive element, and both methods agree to within 3σ in the light frequency range from 437.5-442.5 THz. The interferometric method also yielded a length precision of 10-20 nm. The length measurements also had a frequency dependence, which may have some effects caused by mirror frequency-reflectivity dependence as we explored, but other effects are most likely at play such as the Gouy phase or three-dimensional effects. These effects would need to be addressed to improve the technique.

Optics | Interferometry | Cavity Quantum Electrodynamics

Fabry-Pérot microcavities are of note to study due to their applications in Cavity Quantum Electrodynamics. These cavities are particularly helpful in minimizing mode volume, which can maximize the quantum zero point energy of electromagnetic fields of the cavity modes. In practice, these cavities can be made using optical fibers, which is a special case of these microcavities.

In this project we will be using white light interferometry to measure micron-scale cavity lengths using the reflected spectrum of the cavity. Direct geometrical methods of cavity lengths are insufficient, as they typically have larger fractional errors. Previous work in the subject has an accuracy of 10nm over a range of $100\mu m$ for a similar interferometric technique (1). In addition to analyzing the reflected spectra, transmission spectra could also be used, but are more complicated to handle due to their challenges in the data analysis and experimental setup. Therefore, the reflection technique allows for a simpler setup and the data is relatively easier to handle with Fourier transforms. The object of this project is to lay out the white light interferometry technique, and then compare it with another direct measurement to benchmark the performance.

1. Theory

In this section, the interferometry technique will be laid out, and relevant derivations will be discussed. To begin with, we must first make some assumptions. The first such assumption is that the cavity is one-dimensional, which allows for a simple technique to extract the cavity length from.

A Fabry Pérot cavity is created by two mirrors with an electromagnetic wave that enters between them. This incident wave will have an electric field amplitude of E_0, and the mirrors have reflection and transmission coefficients of r_1, r_2, t_1 and t_2, as well as r_1', r_2'... and so on, where the prime indicates that the field is incident from right to left, otherwise the field is incident from left to right. In Fig. 1, this one-dimensional case is displayed and shows the electric field after each transition.

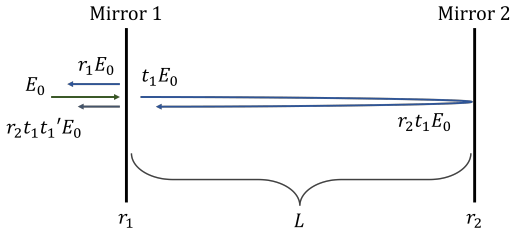

Fig. 1. Electric field transitions for two reflections, one off mirror 1 and one off of mirror 2.

Here we have further assumed normal incidence, and that there are only two reflections (we will revisit this assumption later). In this two-reflection case, the total reflected electric field is given by: $E_r = (r_1 + r_2 t_1 t_1' e^{-i\delta})E_0$, where $\delta = \frac{4\pi L}{\lambda}$ is the optical path difference taken by the field travelling a distance of $2L$. Electric fields are challenging to measure, so the intensity is measured instead. The intensity is given by $I = \frac{1}{2}EE^*$(where E^* is the complex conjugate of E, the electric field), which results in the intensity, I,

$$I = I_0 \left[1 - \left(\frac{t_1 t_1' r_2}{r_1}\right)^2 \cos\left(\frac{4\pi L}{\lambda}\right)\right] \qquad [1]$$

where $I_0 = \frac{1}{2}E_0 E_0^*$.

Under the assumption that there is no frequency dependence on the mirror reflectivities, then for a given input spectrum, $I_{\text{in}}(\omega)$, the reflected spectrum is given as (1):

$$I_R = I_{\text{in}}(\omega)\left[1 - V\cos(\tau_0\omega)\right], \quad \tau_0 = \frac{2L}{c}, \qquad [2]$$

where L is the length of the cavity, $V = \left(\frac{t_1 t_1' r_2}{r_1}\right)^2$ and τ_0 is what we will call the un-shifted travel time in the cavity. This corresponds to the round trip travel time of a photon in the cavity. A spectrometer can measure the intensity of light in different frequencies, giving the spectrum of a cavity. We can extract the cavity length from this by computing the inverse Fourier transform, and if the input spectrum is Gaussian in frequency, then the Fourier transform will have Gaussians in the time domain.

[1]J.S. contributed equally to this work with Y.D.

The idea of the technique is to apply a Gaussian input spectrum, then when taking the inverse Fourier transform, we get three peaks: one centered at $t = 0$, and two centered at $t = \pm\tau_0$. This allows us to extract the cavity length by determining the location of the peak in the time domain. Figures 2 and 3 demonstrate the principle on a simulated example.

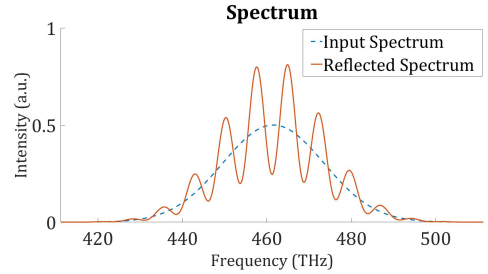

Fig. 2. Example spectrum. In this example, we simulate the input and reflected spectra, where we have assumed the input has a central frequency of $f_0 = 460$ THz and a spectral width of $\Delta f = 12$ THz, as well as a cavity length of $20\mu m$. The mirror reflectivities are set to $r_1 = 1$ and $r_2 = 0.3$. This is then inverse Fourier transformed in Fig. 3.

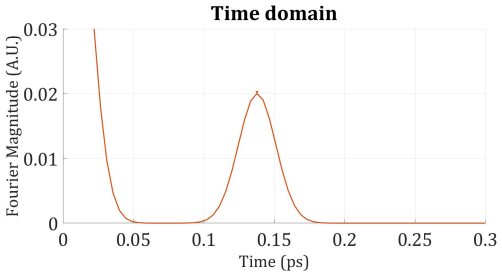

Fig. 3. Inverse Fourier transform of the reflected spectrum in Fig. 2. The peak is loacted at $\tau_0 = 1.338$ ps (using a simple peak finding algorithm), which suggests $L = c\tau_0/2 = 20\mu m$ as expected.

As mentioned earlier, an assumption made was that there are only two reflections. In reality, there are an infinite number of reflections, and the total electric field now has the form (after applying stokes relations, $tt' = (1-r)^2$):

$$E_r = E_0\left[1 + \frac{(1-r_1)^2}{r_1^2}\sum_{n=1}^{\infty}\left(r_1 r_2 e^{-i\tau_0\omega}\right)^n\right] \qquad [3]$$

From this infinite sum, we can see that the two reflection case is just the first term of the series. When we make this an intensity and take the inverse Fourier transform with the same input Gaussian mentioned before, it will result in an infinite number of Gaussians in the time domain located at $t = 0, \pm\tau_0, \pm 2\tau_0, \pm 3\tau_0, ...$, but their amplitudes will decay quickly. This essentially means that we can ignore the higher order terms, as they will be quite small since $r_1, r_2 < 1$. In addition, if the second mirror has a higher reflectivity than the first mirror, then the two reflection case is a good approximation, and the higher order terms can still be truncated to a decent approximation.

2. Materials and Methods

A. Experimental Setup. The interferometer is created using the tip of a fiber (low reflectivity) and a mirror (high reflectivity). In the most general case, the fiber has a curvature which can be created using a laser machining technique similar to Hunger et. al (2) to create radius of curvature on the fiber. To try the technique, we instead used a cleaved fiber with no radius of curvature. The white light laser source is directly coupled into an optical fiber, which is attenuated to reduce the overall power of the laser, such that a spectrometer can be used to measure the spectrum.

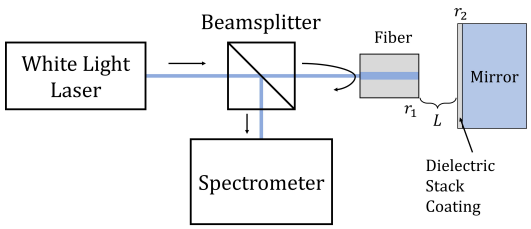

Fig. 4. Experimental setup. All connections use optical fibers to direct the laser, while the cavity is in free space (air). The reflected light is measured with the spectrometer. In addition, the mirror is coated with a dielectric mirror stack.

This setup puts us squarely in the two-reflection regime, as the dielectric mirror has a high reflectivity compared to the fiber to air interface, which has a much lower reflectivity.

To compare the measurement results to another method, a Thor Labs NanoMax 3-axis flexure stage has the fiber attached to it and can precisely move it with a peizoelectric drive element. The NanoMax has a closed loop control mode, which can accurately move and read out micron-level precision. Only one axis was used for the setup, and is controlled using either knobs or a piezoelectric drive element. The piezoelectric drive is controlled with either a closed or open loop voltage source. The element is monitored with another piezoelectric strain sensor to measure the length changes in the drive. For accuracy, the closed loop operation was selected, which maintains the voltage across the piezoelectric drive consistently, while the length is monitored by the strain sensor. Additionally, a microscope is placed on top of the setup so the cavity can be viewed directly. This allowed for monitoring to ensure that the fiber doesn't scratch the mirror and it gives a rough estimate of the length of the cavity.

In order to take data for a given cavity, we first take a reference spectrum. This is used to determine the exact input spectrum, $I_{\text{in}}(\omega)$ to compare with the reflected spectrum. In order to do this, the fiber was manually move to a maximal distance away from the mirror so there is no distinguishable interference. After the reference spectrum was taken, the fiber was moved closer to the mirror, where strong interference was observed and an initial length measurement was taken using the piezoelectric strain sensor and the interferometry method. Aside, the microscope is used to observe the system and make rough order of magnitude measurements of the cavity size. The cavity is then moved closer to the mirror using the piezoelectric drive and another measurement is taken. The change in length of each measurement is noted and compared, and is presented in the results section.

Data Analysis. In order to extract the cavity length from the raw data, a Fourier transform is performed. However, to avoid effects that are caused by background noise in the data, we first subtract the background caused by light in the room. This is done by simply subtracting the background spectrum

from both the input and output spectra when the laser source is off. Then the measured spectrum ($M(\omega)$) is divided by the reference spectrum ($R(\omega)$), and multiplied by a window function ($W(\omega)$). The window function serves to limit the range we are analysing and to weigh the spectrum. The chosen window function is a Gaussian one, centered in a region of interest. This was selected to ensure the data has a Gaussian shape. This removes other effects that would propagate through the Fourier transform. Since the Gaussian has no periodicity associated with it, then it won't affect the shift of the travel time peak in the time domain. The function has the form: $W(\omega) = e^{-\frac{(\omega-\omega_0)^2}{2\Delta\omega^2}}$, where ω_0 is the central frequency of the analysis region, and $\Delta\omega$ is the width of the region. The function allows one to "peer" through a window of a certain area of the data to perform analysis, and allows for us to compare different input spectra on the same cavity length by varying ω_0 and $\Delta\omega$.

Once these pre-processing filters have been applied, we can take the inverse Fourier transform as in equation 4, then fit the data in the time domain to a Gaussian to extract the peak location.

$$i(t) = \mathcal{F}^{-1}\left\{\frac{M(\omega)}{R(\omega)}W(\omega)\right\} \quad [4]$$

This in turn allows us to extract the cavity length from the round trip travel time in the cavity ($\tau_0 = 2L/c$).

Lastly, error propagation can be a bit tricky with taking Fourier transforms. In our case, since the data is discrete, we perform a discrete inverse Fourier transform (DIFT). This can be represented as a square matrix of dimension $N \times N$, where N is the length of the data vector. If the Fourier transform matrix is given as F_N (see (3) for DFT matrix derivation), then the inverse transform is given as:

$$F_{\text{DIFT}} = \frac{F_N^H}{N}, \quad [5]$$

Where F_N^H is the Hermitian conjugate of the complex $N \times N$ Fourier transform matrix, F_N. To propagate the error, we must first construct a covariance matrix for the input data. This matrix is simple, as to a decent approximation, the spectrometer data is not correlated between data values. The spectrometer measures photon counts in each wavelength bin, which are Poissonian in nature. Therefore, if we assume Poissonian counts, then the standard deviation is simply the square root of the counts. Since we further assumed that the spectrometer is not correlated between values, then the covariance matrix, Σ, is of dimension $N \times N$, with the variance of each data point on the diagonal. After performing the Fourier transform, the new covariance matrix, Σ', is then given as:

$$\Sigma' = \frac{1}{N^2}F^H \Sigma F. \quad [6]$$

Since we assumed that the points were uncorrelated in Σ, then we can make the same assumption for Σ', and by taking the diagonals (which are real-valued) we have the variance in the time domain data. This variance can be used to perform a weighted least squares fit on the spectrum data.

3. Results

The results show that there is a good agreement between the NanoMax peizoelectric strain sensor and the interferometric method, within 3σ. Plotted in Fig. 5, we show the technique applied on one cavity length, and then present the results for various changes in length. We observe a linear relationship with a slope near 1, which is as expected if both measurements agree, and the negative slope indicates that we moved the fiber closer to the mirror. These measurements were done with the Gaussian window function mentioned previously, with a central frequency, $f_0 = 440$ THz and a width of $\Delta f = 5$ THz.

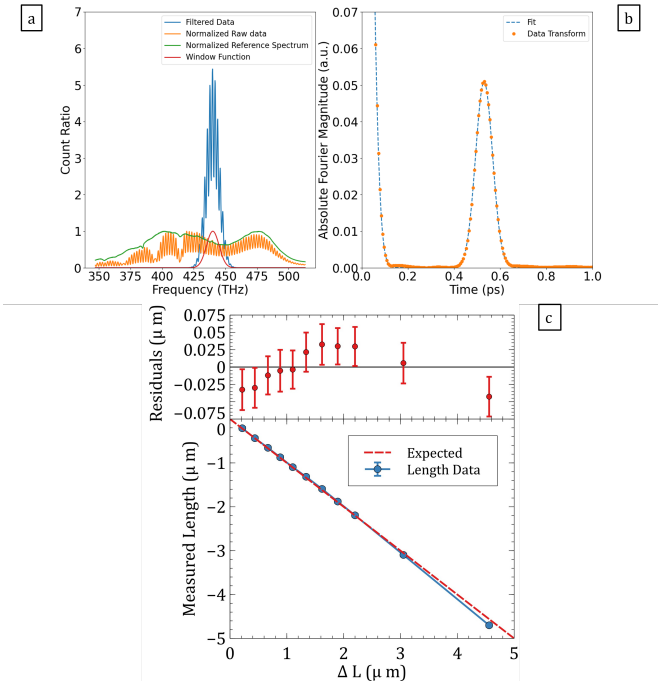

Fig. 5. Experimental results. Figure (a) shows a raw data example from the spectrometer and the filtering process, where we have selected to analyze the region where $f_0 = 440$ THz ($\lambda = 681$ nm) and $\Delta f = 5$ THz. Figure (b) shows the time domain results from taking the inverse fourier transform. The transformed data was fit to a function: $f(t) = A\exp\{t^2\} + B\exp\{b(t-\tau_0)^2\}$ (dotted line). The peak occurs at $\tau_0 = 0.53018(7)$ ps which corresponds to a length of $L = 79.527 \pm 0.007$ μm. Figure (c) shows the extracted length using the technique laid out in a and b, over a range of different lengths. Figures a and b showed the initial length of the cavity, which was used to obtain the measured change in length. The data was fit to a linear function with a slope of -1.03 ± 0.01, which is 3σ within the expected value of -1. Also, $\chi^2_\nu = 1.004$ for 9 degrees of freedom, which indicates a good fit. The residuals show a precision of 10-20 nm.

Mirror Reflectivity Effects

While the results matched well for the case where $f_0 = 440$ THz, we noticed that the results differed in the case of changing the central frequency of the window function. One possible explanation is the wavelength dependence of the mirror reflectivity, which we explore here. If the mirrors have a frequency dependence on the reflectivity, namely $r_1 \to r_1(\omega)$ and $r_2 \to r_2(\omega)$, then the reflected electric field now becomes: $E_r = E_0\left(1 + \frac{r_2(\omega)t_1(\omega)t_1'(\omega)}{r_1(\omega)}e^{-i\delta}\right)$. We can then wrap the reflection and transmission coefficients all under one expression, where $r(\omega) = \frac{r_2(\omega)t_1(\omega)t_1'(\omega)}{r_1(\omega)}$, and then fit a function to it. Since the reflectivity can be complex, then we can perform the following Taylor expansion in the complex exponential:

$$r(\omega) = r_0\exp\left\{i\left[a(\omega-\omega_0) + b(\omega-\omega_0)^2 + ...\right]\right\} \quad [7]$$

For two terms of the Taylor expansion, the intensity becomes:

$$I_R(\omega) = I_{in}(\omega)[1 + 2r_0(r_0 - 1) - r_0(r_0 - 1)\times (e^{-i\tau_0\omega - ia(\omega-\omega_0) - ib(\omega-\omega_0)^2} + e^{i\tau_0\omega + ia(\omega-\omega_0) + ib(\omega-\omega_0)^2})] \quad [8]$$

When taking the inverse Fourier transform, the first two linear terms with r_0 don't affect the peak in the time domain. The linear term in the complex exponential (parameter a) will be responsible for shifting the peak compared to having no frequency dependence in the reflectivity. This shift is simply $\tau = \tau_0 + a/2\pi$, where τ is the new peak location, and τ_0 is the "naive" assumption, $\tau_0 = 2L/c$. This results in a new equation for the length, for a measured τ and given parameters a and b (which is our correction for the length):

$$L = \frac{c}{2}\left[\tau - \frac{a}{2\pi}\right] \quad [9]$$

This shift is demonstrated numerically in Fig. 6, where a 20 μm cavity is compared to one with a frequency dependent mirror reflectivity.

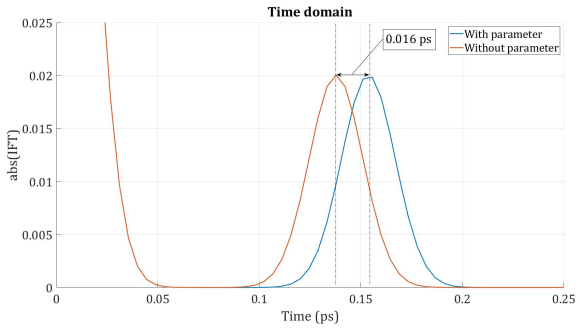

Fig. 6. Simulated cavity numerical example where $r(\omega) = 0.3e^{ia\omega}$ for parameter $a = 1 \times 10^{-13}$ rad · s. The cavity was set at $L = 20$ μm, corresponding to $\tau_0 = 0.138$ ps, which is the orange plot (unshifted where $a = 0$). The blue plot corresponds to a shift in the peak of about 0.016 ps. The shifted peak appears at $\tau = 0.154$ ps.

In the Experimental setup, we can make an approximation that the frequency dependence is dominated by the dielectric mirror stack. This results in $r(\omega) \approx r_{\text{mirror}}(\omega)$, which simplifies analysis. The method of obtaining $r(\omega)$ will be discussed in the next section.

Looking at the experimental result over different frequencies for a single cavity length, we can see how the length is affected by the frequency we choose. The relationship is shown in Fig. 7.

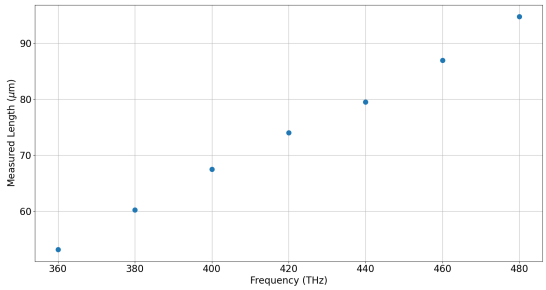

Fig. 7. Frequency dependence of the "naive" length measurement using τ_0 (not taking into account frequency dependence of reflectivity). The cavity length is kept constant here, but the region of analysis is kept at $\Delta f = 5$ THz with the plotted central window function frequencies, f_0. Only one dataset is selected here, which was the initial length measurement reported in the example in Fig. 5 a and b.

From Fig. 7, we observe a linear relationship between the frequency selected and the measured length for the same cavity length. This shows that there is a frequency dependence on our measurements. In order to handle the frequency dependence, we propose a technique to fit the reflection coefficients to equation 7 of the dielectric mirror stack used, then apply corrections to the length using the linear parameter, a, mentioned before. In order to obtain these values we use the transfer matrix method to simulate the wavelength dependence of the mirror reflectivity, then fit a function to the phase parts. The next section will cover how the transfer matrix method works and how we fit the parameters.

Transfer Matrix Calculations. In order to handle the specific mirror used in the lab, we employed the transfer matrix method to fit $r(\omega)$ from equation 7. A MATLAB program was implemented to generate the reflection coefficients given the manufacturer specifications of the mirror stack, which is made of several layers of alternating indices of refraction. Assuming normal incidence, the stack is represented using the following matrices (derivation in (4)):

$$M_{i,j} = \frac{1}{2n_i}\begin{pmatrix} n_i + n_j & n_j - n_i \\ n_j - n_i & n_i + n_j \end{pmatrix}, \quad [10]$$

$$T_i = \begin{pmatrix} e^{i2\pi n_i d_i/\lambda} & 0 \\ 0 & e^{-i2\pi n_i d_i/\lambda}, \end{pmatrix} \quad [11]$$

where n_i is the index of layer i, and d_i is the thickness of the layer. $M_{i,j}$ is the layer interface matrix, which handles the reflections from one layer to the next. T_i is the propagation matrix which accounts for the optical path length picked up by the electric field travelling the length of the layer. These matrices are multiplied to get the combined matrix for a stack with N layers, and the stack has an entry index of refraction, n_a and exit index of refraction, n_b:

$$M_{tot} = M_{N,b}T_N M_{N-1,N}...M_{2,1}T_1 M_{a,1} \quad [12]$$

After computing the combined matrix, M, the transmission and reflection coefficients are given by the relation:

$$\tilde{r} = -\frac{M_{21}}{M_{22}},\ \tilde{t} = M_{11} - \frac{M_{12}M_{21}}{M_{22}}, \quad [13]$$

where $\tilde{r}$ and $\tilde{t}$ are allowed to be complex. Fig. 8 shows the frequency dependence of the mirror stack on the reflection coefficient, $R = |r|^2$ and the phase shift.

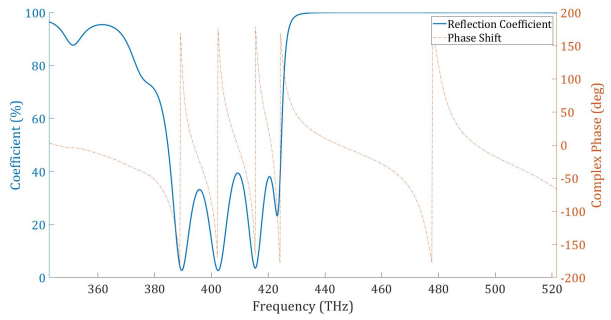

Fig. 8. Frequency dependence of the dielectric mirror stack. The reflection percentage is defined as $R = 100 \cdot |\tilde{r}|^2$ from equation 13, and the phase is the complex angle. The layer dimensions and indices of refraction were provided by the manufacturer of the mirror.

From the phase plot, we can then extract the parameters a, b and ω_0 from equation 7. The fitting technique uses the same window function mentioned in the data analysis section, which uses Gaussian weights to fit to the region of analysis. This results in an approximation for the phase changes over the region of analysis. In addition, the phase is "unwraped" such that it is not limited to $\pm 180°$, but is allowed to have values beyond. This removes the asymptotes observed in the phase from Fig. 8.

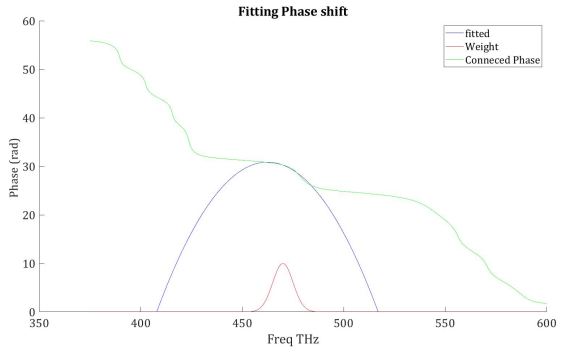

Fig. 9. Fitting the Phase for the dielectric mirror

Applying these corrections to the experimental data yields some improvement on the consistency of the measurement. Fig. 9 shows the results corrected for the frequency dependence on the reflectivity.

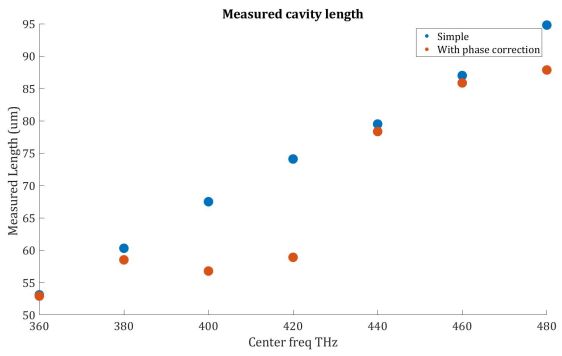

Fig. 10. Length correction accounting for phase of the dielectric mirror

We can see in Fig. 10 that the corrections are evening out the measurements on the range from $360 - 420$ THz, which is expected. However, on the range from $440 - 480$ THz the corrections hardly affect the measurement. This is unexpected, as in Fig. 9 we can see that the nicely linear region occurs at around $420 - 480$ THz, which we expect would correct the measurements better. This is not what we see from the results, which suggests there is another effect at play.

Another effect to handle comes from the one-dimensional assumption. If we instead observe the slope from the displacement plot (as in Fig. 5), but change the central window function frequency, and their slopes don't match, then there is another effect at play. We plot these in Fig. 11, where a clear trend appears as the slope increases when the central frequency increases.

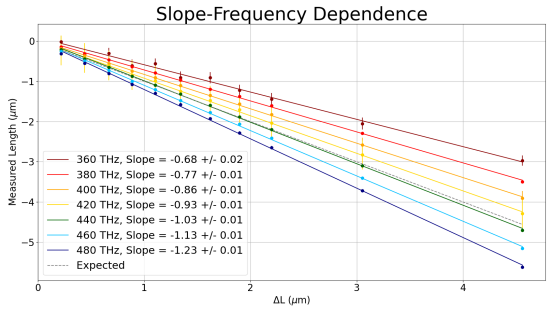

Fig. 11. Frequency Dependence on the slope. The central analysis frequency (f_0 from the window function) was swept from $360 - 480$ THz, and the same analysis was performed as in Fig. 5. As in the aforementioned figure, the expected slope is -1 for both the NanoMax and interferometry methods to agree.

The effects most likely to obtain this result can be attributed to the three-dimensional geometry of the cavity. Introducing angles (i.e. no normal incidence) adds another set of frequency dependent effects. The transfer matrix method, as well as the one-dimensional cavity assumptions break down, and require adding angular dependencies to handle those cases. In addition, we have not taken into account the shape of the laser beam, namely the Gaussian nature of the beam, which induces its own set of considerations to handle.

4. Discussion

In the first part of the results, where we took the "naive" assumption, and found a frequency region where the displacements match with the NanoMax piezoelectric drive stage. However, upon inspection over different frequencies, we found the cavity length measurement has a frequency dependence.

While the corrections did make some of the measurement more consistent on the measurement range, there is still some work to be done. We are not sure why the correction does not work above 440 THz. A direction for exploring this issue is to simulate data using our mathematical model and see if it has the same results. Another potential cause of the discrepancies over the frequency range can be attributed to the Gouy Phase from a Gaussian beam. If we assume the white light source is a Gaussian beam, we can apply further corrections. While not explored here, it may be worth looking into for further

improvements. To illustrate, the Gouy Phase for the cavity is:

$$\phi(\omega) = \arctan\left(\frac{4Lc}{w_0^2}\frac{1}{\omega}\right), \qquad [14]$$

where w_0 is the beamwaist of the Gaussian beam. However, now the length of the cavity appears in the term and would have its own challenges to handle.

Other effects to explore would be geometrical effects that arise from three-dimensional geometry (since we assumed one dimension). Fig. 11 shows that some effects from three-dimensional geometry need to be taken into account. For instance, if the angle between the fiber and mirror changes, or if the mirrors and cavity are not flat, then these would have to be taken into consideration. Other effects from the three-dimensional nature of Gaussian beams would come into play to account for.

5. Conclusion

This paper showed our method of using white light interferometry to measure a Fabry Pérot cavity. The length measurement is compared with a piezoelectric drive element, and both methods agree to within 3σ in the light frequency range from $437.5 - 442.5$ THz. However, measured lengths change with the frequency of the input source. We sought to account for this by the phase change of reflectivity of the dielectric mirror, which helped for parts of the frequency spectrum.

More work needs to be done to optimize the length measurement of the cavity consistently for all input spectra. If this method is improved it would be a convenient, accurate, and precise way of measuring cavity lengths. Since the measurements don't take much time and the Fourier transform can be optimized, then this method can be quicker to employ than other traditional methods, even allowing for real-time monitoring of cavity lengths. Additionally, effects of objects in the cavity can be explored to probe more complicated systems using this technique.

ACKNOWLEDGMENTS. Thanks to Lilian Childress for taking us on this project. Thanks to Rigel Zifkin for his help in the lab and with some concepts of the technique.

References

1. LM Manojlović, A simple white-light fiber-optic interferometric sensing system for absolute position measurement. *Opt. Lasers Eng.* **48**, 486–490 (2010).
2. D Hunger, et al., A fiber fabry–perot cavity with high finesse. *New J. Phys.* **12**, 065038 (2010).
3. KR Rao, KR Rao, PC Yip, IW Selesnick, G Schuller, *Chapter 2: The Discrete Fourier Transform.* (CRC Press), p. 57–98 (2001).
4. BEA Saleh, MC Teich, *Chapter 7: Photonic Crystal Optics.* (Wiley), 3 edition, p. 255–302 (2019).